iScience

Article

Local keratinocyte-nociceptor interactions enhance obesity-mediated painful small fiber neuropathy via NGF-TrkA-PI3K signaling axis

Graphical abstract

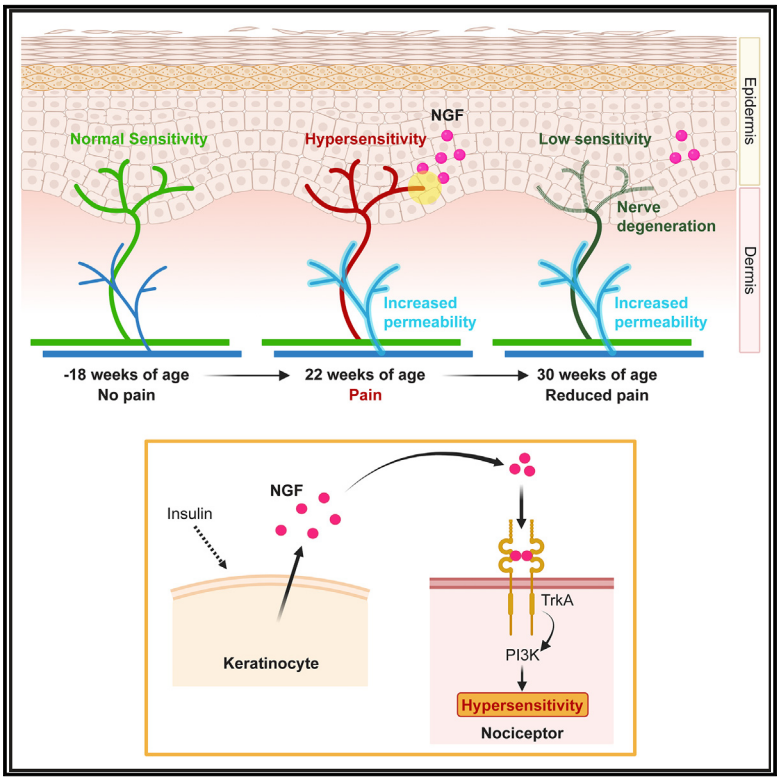

Highlights

- DIO enhances pain-associated behaviors and sensory hypersensitivity in the skin
- Pain behaviors and sensory hypersensitivity are followed by axon degeneration
- DIO enhances the expression of NGF in keratinocytes via insulin signaling
- Keratinocyte-derived NGF is responsible for hypersensitivity of skin sensory axons

Authors

Yuta Koui, Shuxuan Song, Xinzhong Dong, Yoh-suke Mukouyama

Correspondence

mukoyamay@mail.nih.gov

In brief

Cell biology; Human metabolism

Koui et al., 2025, iScience *28*, 112047
March 21, 2025 Published by Elsevier Inc.
https://doi.org/10.1016/j.isci.2025.112047

CellPress

iScience

CellPress
OPEN ACCESS

Article

Local keratinocyte-nociceptor interactions enhance obesity-mediated painful small fiber neuropathy via NGF-TrkA-PI3K signaling axis

Yuta Koui,[1] Shuxuan Song,[1,2] Xinzhong Dong,[3,4] and Yoh-suke Mukouyama[1,5,*]

[1]Laboratory of Stem Cell and Neuro-Vascular Biology, Cell and Developmental Biology Center, National Heart, Lung, and Blood Institute, National Institutes of Health, Bethesda, MD 20892, USA

[2]Biological Sciences Graduate Program, University of Maryland, College Park, MD 20742, USA

[3]The Solomon H. Snyder Department of Neuroscience, Johns Hopkins University School of Medicine, Baltimore, MD 21205, USA

[4]Howard Hughes Medical Institute, Johns Hopkins University School of Medicine, Baltimore, MD 21205, USA

[5]Lead contact

*Correspondence: mukoyamay@mail.nih.gov

https://doi.org/10.1016/j.isci.2025.112047

SUMMARY

The pathology of painful small fiber neuropathy, characterized by neuropathic pain and axon degeneration, develops locally within the skin during the stages of obesity and pre-diabetes. However, the initiation and progression of morphological and functional abnormalities in skin sensory nerves remains elusive. We evaluated pain-associated wiping behavior and conducted *ex vivo* live Ca^{2+} imaging of the diet-induced obesity (DIO) ear skin to detect sensory hypersensitivity. Our findings reveal sensory hypersensitivity in skin nociceptive axons followed by axon degeneration. Further mechanistic analysis identified keratinocytes as a major source of nerve growth factor (NGF) in DIO skin, which locally sensitizes nociceptors through NGF and its receptor tropomyosin receptor kinase A (TrkA)-mediated downstream signaling, including the phosphoinositide-3-kinases (PI3K) pathway. Thus, targeting these local interactions between keratinocytes and nociceptors offers a therapeutic strategy for managing neuropathic pain, avoiding the adverse effects associated with systemic interventions.

INTRODUCTION

Neuropathy is one of the most common complications of diabetes and affects approximately 50% of patients with diabetes during the course of their disease. A subset of patients in the early stage of diabetes, including obesity or pre-diabetes, develop neuropathic pain in the skin of peripheral tissues, such as legs and hands, known as painful small fiber neuropathy.[1–3] The primary symptoms of painful small fiber neuropathy include burning or lancinating pain in the skin,[4] a reduction in intraepidermal nerve fibers,[5] morphological changes in proximal nerves and dorsal root ganglions (DRGs),[6,7] often accompanied by abnormal dermal capillaries.[8–10] These symptoms are well characterized in human patients, but the sequential process of pathogenesis and correlation between symptoms remains unclear. Given that neuropathic pain is thought to be an early symptom of painful small fiber neuropathy,[3] the mechanism underlining the initiation and progression of a painful sensation in skin nociceptive nerves needs to be investigated for further prevention of severe neuropathy including painless neuropathy in patients with severe diabetes. Considering that the etiology and pathogenesis of painful small fiber neuropathy are presently thought to be influenced by systemic hyperglycemia, dyslipidemia, and insulin resistance, the precise mechanism through which local aberrant signals impact the pathophysiological processes of painful small fiber neuropathy in the skin remains unclear.

Previous studies employing diabetic mouse models successfully recapitulated the pathologies of painful small fiber neuropathy, including mechanical allodynia and axon degeneration in the footpad skin, abnormal hypersensitivity in DRG sensory neurons, and vascular abnormalities in sciatic nerves.[8,10–12] However, the mechanisms underlying the initiation and progression of morphological and functional abnormalities in sensory axons and capillaries within the skin of the diabetic mouse models are still inconclusive. Since neuropathic pain and small fiber degeneration are thought to occur during the stages of obesity and pre-diabetes,[13–15] we employed mouse ear skin to address the underlying mechanisms of painful small fiber neuropathy in mice with diet-induced obesity (DIO), the mouse models for obesity and pre-type 2 diabetes. We developed a behavioral assay in which capsaicin application elicits pain-associated wiping behavior of the ears. This was combined with primary sensory neuron-specific GCaMP3 Ca^{2+} imaging to detect hypersensitivity of peripheral terminals of nociceptive neurons in the skin of the ears. Our studies not only reveal the pathogenesis of painful small fiber neuropathy in the DIO ear skin but also uncover the dominant role of keratinocyte-nociceptor interactions via nerve growth factor (NGF)-tropomyosin receptor kinase A (TrkA)-phosphatidylinositol

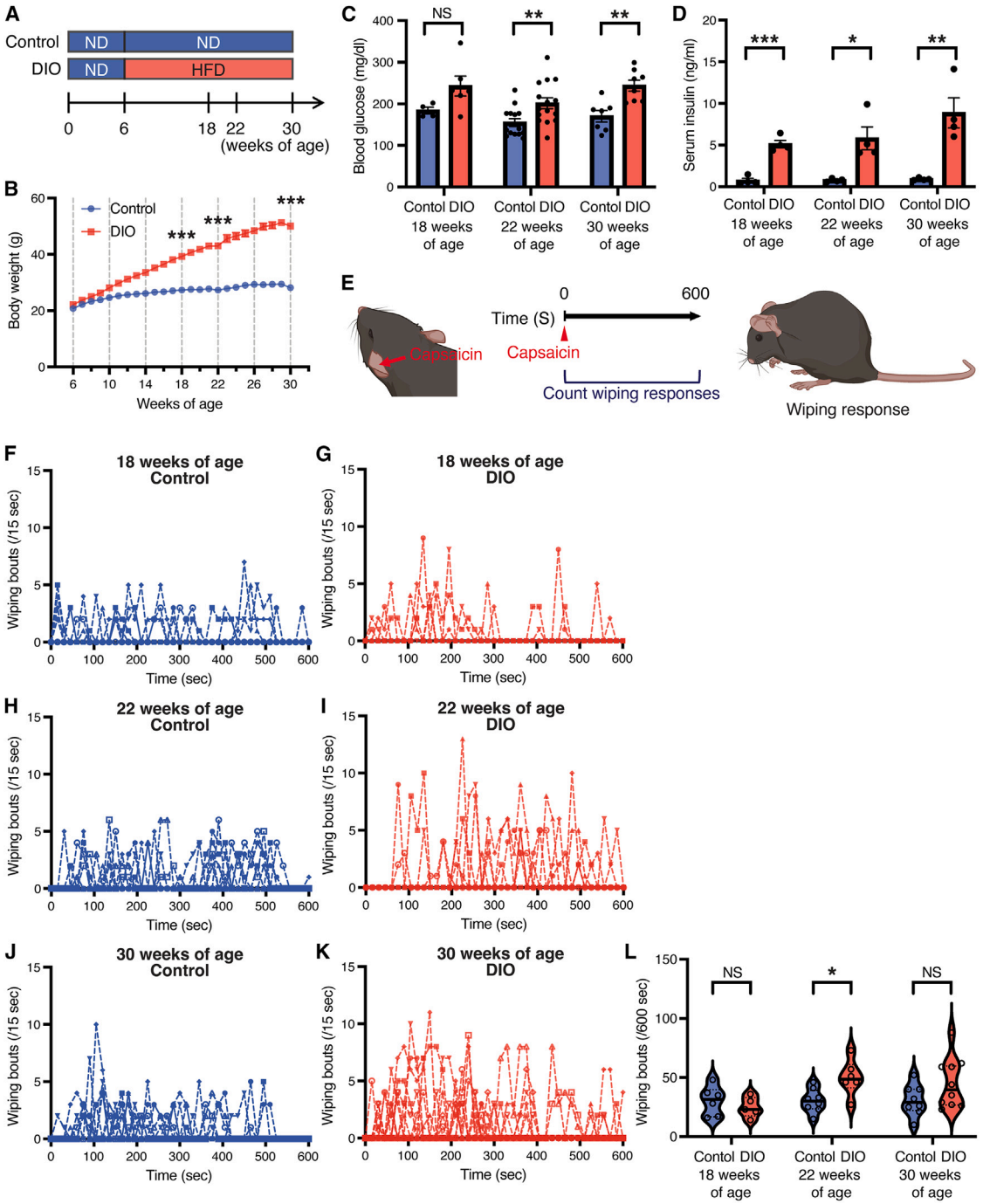

Figure 1. DIO enhances pain-associated behavior in mice

(A) Schematic diagram of the induction of diet-induced obesity (DIO) in mice. Mice were fed either a high-fat diet (HFD) to induce DIO or a normal diet (ND) for control from 6 to 30 weeks of age.

(B) Body weights of control (N = 33) and DIO (N = 38) mice from 6 to 30 weeks of age.

(C) Blood glucose levels for both control and DIO mice at 18, 22, and 30 weeks of age (N = 4, 14, 7 control; N = 6, 15, 8 DIO at 18, 22, and 30 weeks of age, respectively).

(D) Serum insulin levels for both control and DIO mice at 18, 22, and 30 weeks of age (N = 4, 4, 4 control; N = 4, 4, 4 DIO at 18, 22, and 30 weeks of age, respectively).

(E) Illustrations depicting the capsaicin-mediated acute pain behavior assay in mouse ear skin: Capsaicin was applied to the skin behind the ears (the outer layer of the ear skin) of both control and DIO mice. Forelimb wiping responses were recorded for 600 s following capsaicin application.

(legend continued on next page)

3-kinase (PI3K) signaling within the epidermis in sensitizing peripheral terminals of nociceptive neurons.

RESULTS

Diet-induced obesity enhances pain-associated behavior in mice

Male mice were fed a high-fat diet from 6 to 30 weeks of age to develop DIO (Figure 1A). Mice with a high-fat diet exhibited a significant increase in body weight from 18 weeks of age (high-fat diet for 12 weeks) onward (Figure 1B). Blood glucose and serum insulin levels gradually increased from 18 weeks of age and were significantly upregulated from 22 weeks of age (high-fat diet for 16 weeks) onward (Figures 1C and 1D). To initially assess the link between pain-associated behavior and hypersensitivity of peripheral terminals of nociceptive neurons in the skin of mice with obesity or pre-diabetes, we chose to utilize the ear skin of DIO mice due to its simple structure, thin layer, and high accessibility. Capsaicin, a ligand for transient receptor potential vanilloid subtype 1 (TRPV1) channel, was applied to the skin behind the ears (the outer layer of the ear skin) of both control and DIO mice (Figure 1E). Since the noxious pain stimuli evoke forelimb wiping responses,[16,17] we counted those responses for 600 s after the capsaicin application (Figure 1E). No wiping responses were observed in both control and DIO mice before capsaicin application (data not shown), suggesting no difference in spontaneous ongoing pain between control and DIO mice at each stage. Despite the capsaicin application evoking forelimb wiping responses at the stimulus site of ear skin in both control and DIO mice, the wiping bouts were significantly increased in DIO mice at 22 weeks of age (Figures 1F–1L). At 30 weeks of age (high-fat diet for 24 weeks), the wiping bouts were slightly enhanced in DIO mice; however, there was a large dispersion between replicates, and no significant difference was observed between control and DIO mice (Figures 1J–1L). Taken together, DIO did not enhance the capsaicin-mediated pain-associated behaviors at 18 weeks of age; however, it did enhance these pain behaviors at 22 weeks of age. At 30 weeks of age, the enhanced pain behaviors were attenuated.

Diet-induced obesity triggers sensory hypersensitivity followed by skin axon degeneration

We next measured the sensitivity of peripheral terminals of nociceptive neurons in the epidermis of the ear skin using *Pirt-GCaMP3* calcium indicator mice, in which *GCaMP3* is driven by the sensory neuron-specific *Pirt* promoter.[18] We dissected the outer layer of the ear skin from *Pirt-GCaMP3* mice for *ex vivo* live Pirt-GCaMP3 Ca^{2+} imaging of the ear skin explants (Figure S1A). We conducted imaging of branched sensory axon and terminal activation in response to 2 μM and 10 μM capsaicin applications, based on GCaMP3 fluorescence within the center region of the ear skin epidermis at a depth of 20 μm (Figures S1A and S1B). After capturing time-lapse Pirt-GCaMP3 Ca^{2+} images for 600 s, individual axons were selected from each image for quantification: Ca^{2+} transient ($\Delta F/F_0$) in each selected axon and the area under the curve (AUC) for the integrated Ca^{2+} elevation which indicates the total sensory activity in response to nociceptive stimuli were then quantified (Figures S1C–S1E). At 18 weeks of age, 2 μM capsaicin application did not show any significant difference in Ca^{2+} responses in sensory axons within the ear skin explants between control and DIO mice. However, 10 μM capsaicin application evoked higher Ca^{2+} responses in the ear skin explants from DIO mice compared to controls (Figures 2A–2D and S2A–S2D). These results suggest that sensory hypersensitivity is not fully developed in DIO skin at 18 weeks of age. At 22 weeks of age, both 2 μM and 10 μM capsaicin applications evoked higher Ca^{2+} responses in the ear skin explants from DIO mice compared to controls, suggesting that sensory hypersensitivity is fully developed in DIO ear skin at 22 weeks of age (Figures 2E–2H and S2E–S2H). At 30 weeks of age, 2 μM capsaicin application did not show any significant difference in Ca^{2+} responses in the ear skin explants between control and DIO mice. Conversely, 10 μM capsaicin applications attenuated Ca^{2+} responses in the ear skin explants from DIO mice compared to controls (Figures 2I–2L and S2I–S2L). Collectively, the *ex vivo* live Pirt-GCaMP3 Ca^{2+} imaging of the ear skin explants from DIO mice demonstrated that the capsaicin-mediated sensory hypersensitivity peaked at 22 weeks of age, followed by a subsequent attenuation at 30 weeks of age. This hypersensitivity in the epidermis of the ear skin corresponds to the forementioned capsaicin-mediated pain behaviors. A high level of KCl activated branched sensory axons and terminals, but did not show any significant difference in Ca^{2+} responses in the ear skin explants between control and DIO mice at 22 weeks (Figures S2M and S2N). These data suggest that hypersensitivity in DIO sensory axons at 22 weeks of age is caused by nociceptive stimulus-dependent TRPV1 hypersensitivity.

The observation that hypersensitivity was attenuated at 30 weeks of age, along with the reduction in pain-associated behaviors, prompted us to examine whether these attenuations result from axon degeneration in nociceptive neurons within the epidermis of the ear skin, a hallmark symptom of painful small fiber neuropathy. Indeed, Pirt-GCaMP3 Ca^{2+} imaging at 30 weeks of age indicated a reduction in axon length within the epidermis of DIO ear skin compared to controls (Figure 3Q), whereas at both 18 and 22 weeks of age, there was no significant difference observed in axon length between control and DIO ear skin (Figures 3A and 3I). Similarly, our section immunohistochemical analysis of control and DIO ear skin clearly showed a significant reduction in intraepidermal nerve fiber (IENF) density, quantified by the number of nerve fibers crossing the epidermal-dermal junction, in DIO ear skin at 30 weeks of age (Figures 3R–3X), whereas at both 18 and 22 weeks of age, there was no significant difference in the IENF density between control and DIO

(F–K) Forelimb wiping responses following capsaicin application in both control (F, H, and J) and DIO (G, I, and K) mice at 18 weeks of age (F, $N = 6$ control; G, $N = 5$ DIO), 22 weeks of age (H, $N = 8$ control; I, $N = 6$ DIO), and 30 weeks of age (J, $N = 8$ control; K, $N = 10$ DIO). Each dot represents wiping bouts per 15 s
(L) Violin plots showing total forelimb wiping responses following capsaicin application in both control and DIO mice at 18, 22, and 30 weeks of age. Results are shown as the mean ± SEM (C, D, and E). $^{*}p < 0.05$, $^{**}p < 0.01$, $^{***}p < 0.001$; NS, not significant ($p > 0.05$). p values were determined by the parametric two-tailed t test. The schematic diagrams were partially created with BioRender.com.

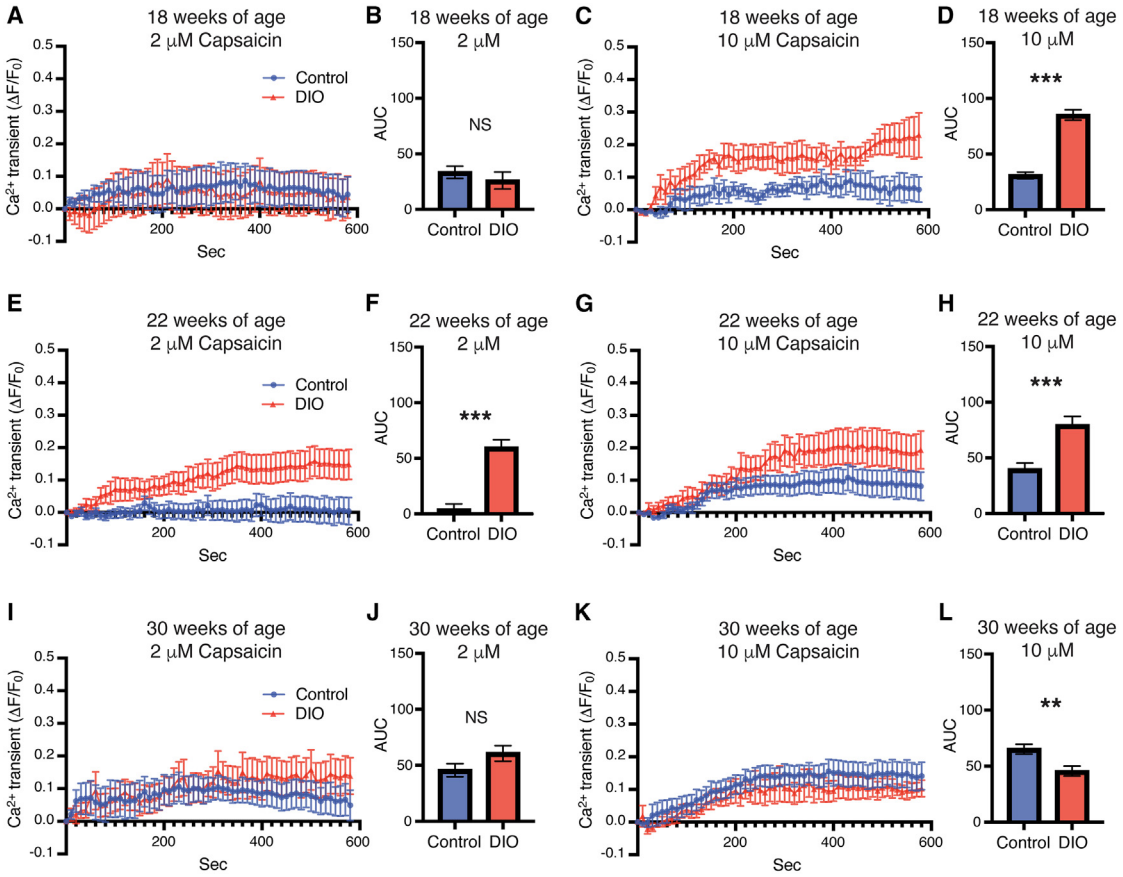

Figure 2. DIO induces sensory hypersensitivity within the epidermis

(A–L) Quantification of Ca^{2+} responses within the ear skin explants from *Pirt-GCaMP3* control (blue) and DIO (red) mice at 18 weeks of age (A-D, $N = 4$ control, $N = 5$ DIO), 22 weeks of age (E-H, $N = 12$ control, $N = 12$ DIO), and 30 weeks of age (I-L, $N = 6$ control, $N = 7$ DIO). The amplitude of the Ca^{2+} transient was evoked by 2 μM capsaicin (A, E, and I) and 10 μM capsaicin (C, G, and K). Ca transient was normalized by baseline Ca^{2+} transient ($\Delta F/F_0$). The integrated Ca^{2+} transient ($\Delta F/F_0$) was calculated as the area under curve (AUC) (B, D, F, H, J, and L). See also Figures S1 and S2. Results are shown as the mean ± SEM. $^{**}p < 0.01$, $^{***}p < 0.001$; NS, not significant ($p > 0.05$). *p* values were determined by the parametric two-tailed *t* test.

ear skin (Figures 3B–3H and 3J–3P). Collectively, these data suggest that DIO ear skin develops sensory hypersensitivity before axon degeneration.

We further examined morphological changes in sensory nerves and blood vessels in DIO ear skin (Figures S3A and S3B). Previously, we demonstrated the co-branching of sensory nerves and large-diameter blood vessels covered by vascular smooth muscle cells (VSMCs) in the deep dermis of ear skin.[19] At 22 and 30 weeks of age, no significant changes were observed in the branching patterns of sensory nerves and blood vessels in the deep dermis between control and DIO ear skin (Figures S4A–S4T). Additionally, there were no significant changes found in VSMC coverage of large-diameter blood vessels (Figures S4A–S4T) or myelination of sensory nerves (Figures S4U–S4Z) between control and DIO ear skin. In contrast, given that skin capillary endothelial cells form non-fenestrated blood vessels with adhesion junctions between endothelial cells,[20] we observed the increased expression of the vascular hyperpermeability marker, plasmalemma vesicle-associated protein (PLVAP),[21] in DIO skin vasculature adjacent to the boundary between the epidermis and dermis at 22 and 30 weeks of age, but not 18 weeks of age (Figures S5A–S5U). These data suggest that the timing of the emergence of vascular permeability in the skin vasculature coincides with the development of sensory hypersensitivity in DIO mice. Given that immune cells are known to modulate nociceptor terminals in the pathological skin,[22] we observed no significant change in the number of $CD45^+$ immune cells within the epidermis of DIO ear skin, where hypersensitivity in sensory axon terminal was detected (Figures S5V–S5B′).

Diet-induced obesity enhances the expression of nerve growth factor, sensitization of nociceptors, in the epidermis

Neurotrophic factors support the growth, differentiation, and maintenance of neuronal cells in development, but they also contribute to neurological disorders in both peripheral and central nervous systems.[23] In chronic diseases, among those neurotrophic factors, NGF is known to promote pain reactions in sensory nerves by inducing TRPV1 expression, facilitating TRPV1 trafficking to cell membrane, or sensitizing

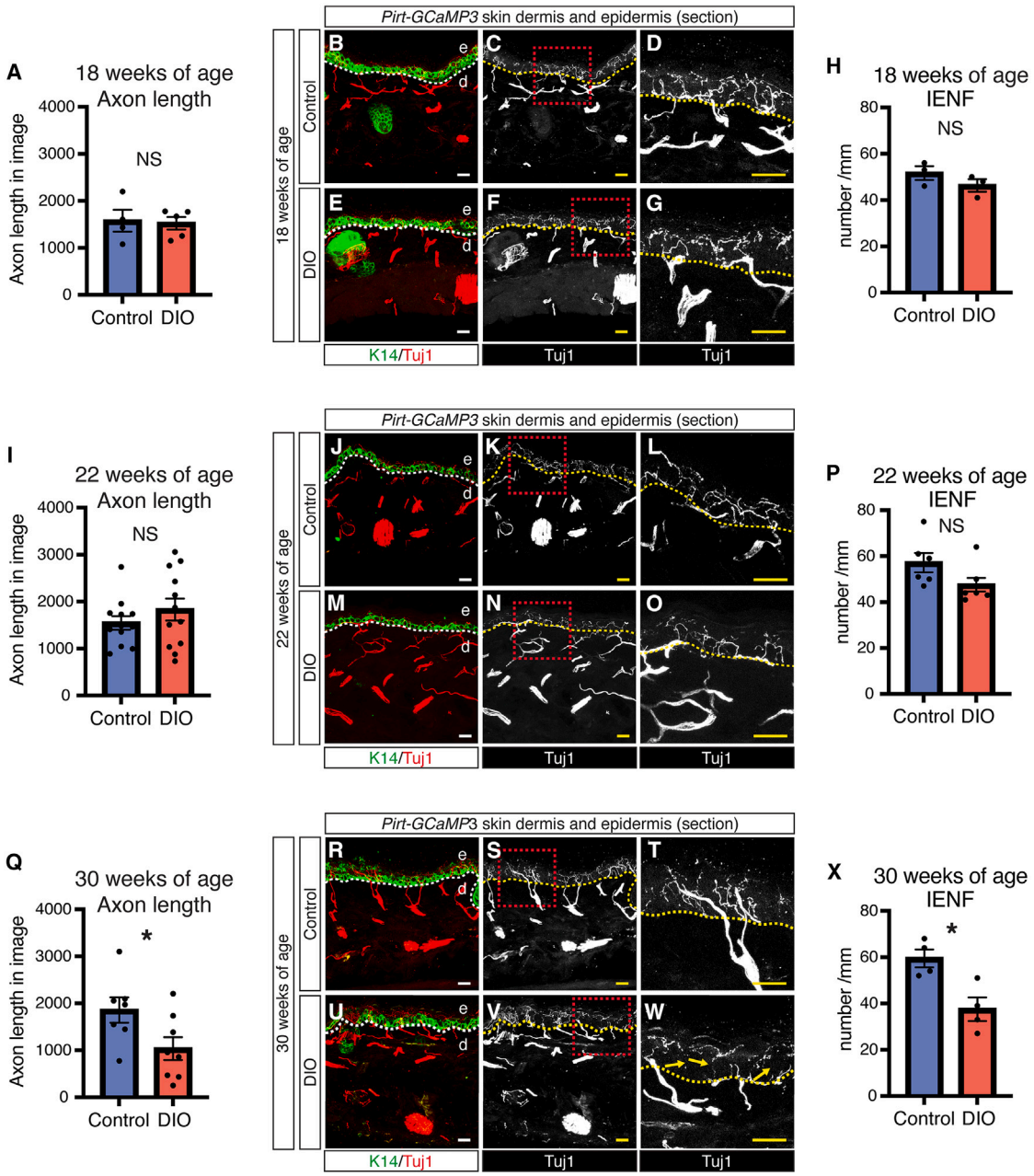

Figure 3. DIO induces skin axon degeneration within the epidermis

(A, I and Q) Total length of GCaMP3-expressing axons in the epidermis at 18 weeks of age (A, $N = 4$ control, $N = 5$ DIO), 22 weeks of age (I, $N = 12$ control, $N = 12$ DIO), and 30 weeks of age (Q, $N = 7$ control, $N = 8$ DIO).

(B–G, J–O, and R–W) Representative images of double-immunofluorescence staining of ear skin sections of *Pirt-GCaMP3* control (B-D, J-L, and R-T) or DIO (E-G, M-O, and U-W) mice at 18, 22, and 30 weeks of age. Antibodies to the keratinocyte marker K14 (green) and the pan-axon/neuron marker neuron-specific class III β-tubulin (Tuj1, red or white) were used. The dotted box regions in (C), (F), (K), (N), (S), and (V) were magnified in (D), (G), (L), (O), (T), and (W), respectively. Dashed lines indicate the border between the epidermis (e) and the dermis (d). Yellow arrows in (W) indicate degenerated axons in the epidermis. Scale bars: 20 μm

(H, P, and X) Quantification of intraepidermal nerve fibers (IENF) in each image at 18 weeks of age (H, $N = 3$ control, $N = 3$ DIO), 22 weeks of age (P, $N = 6$ control, $N = 6$ DIO), and 30 weeks of age (X, $N = 4$ control, $N = 4$ DIO). The linear IENF density is calculated and expressed as the number of fibers per millimeter of epidermal length (IENF/mm). See also Figures S3, S4, and S5. Results are shown as the mean ± SEM. $^*p < 0.05$; NS, not significant ($p > 0.05$). p values were determined by the parametric two-tailed t test.

TRPV1 receptor.[24–28] Although lower NGF expression in epidermal keratinocytes isolated from patients with severe diabetes has been reported,[29] its expression and function in the epidermis of patients with obesity and pre-diabetes having painful small fiber neuropathy has not been examined yet. To address whether NGF affects the sensitization of peripheral terminals of nociceptive neurons in the epidermis of ear skin, we initially examined NGF expression in the epidermis from control and DIO ear skin at 22 weeks of age. Among the three neurotrophic factors tested, we observed increased expression of *Ngf* in the epidermis of DIO ear skin compared to control, whereas no significant changes were detected in the expression levels of *Bdnf* and *Ntf3* (Figure 4A). In support of this result, Pirt-GCaMP3^{+} sensory nerves in the epidermis express NGF receptor, TrkA, but not TrkB and TrkC (Figures S6A–S6I).

We next addressed whether the onset of NGF expression in the epidermis correlates with the development of sensory hypersensitivity in DIO mice (Figure 4B). At 22 weeks of age, X-gal staining of ear skin sections from *NGF-LacZ* mice showed increased expression of NGF in the epidermis of DIO ear skin compared to control (Figures 4C and 4D). For quantification measurements, we further validated the enhanced NGF expression in the epidermis of DIO ear skin using a fluorescent version of LacZ detection, SPiDER-βgal staining in conjunction with the keratinocyte markers K10 and K14 (Figures 4E-4R). In contrast, at 18 weeks of age, we did not observe any significant difference in NGF expression in the epidermis between control and DIO ear skin (Figures S7A–S7O and 4S). At 30 weeks of age, there was a significant difference in NGF expression in the epidermis between control and DIO ear skin, albeit with a reduced expression level compared to that at 22 weeks of age (Figures S7P–S7D′ and 4S). We should note that dermal NGF expression was primarily detected in VSMCs of large-diameter blood vessels, as observed through whole-mount X-gal or SPiDER-βgal staining. However, no significant differences were observed in the expression levels between control and DIO ear skin, nor between those different stages (Figures S8A–S8X). Collectively, at 22 weeks of age, both increased NGF expression and the development of sensory hypersensitivity were observed in the epidermis of DIO ear skin.

We then examined what controls NGF expression in the epidermis. Considering that keratinocytes constitute over 95% of the cells in the epidermis, we initially isolated keratinocytes from the ear skin of adult mice, cultured them with glucose, insulin, or a combination of both, and subsequently assessed *Ngf* expression (Figures 4T and 4U). A high level of insulin enhances *Ngf* expression in primary keratinocytes in culture, whereas a high level of glucose did not show any inductive effect on its expression (Figure 4U). These data suggest that epidermal keratinocytes are a major source of NGF in response to increased levels of insulin in DIO ear skin.

Inhibition of nerve growth factor-tropomyosin receptor kinase A-phosphoinositide-3-kinase signaling suppresses sensory hypersensitivity in the skin of diet-induced obesity mice

To address whether NGF-TrkA signaling is necessary for the sensitization of peripheral terminals of nociceptive neurons in the epidermis of DIO ear skin, we pre-treated the ear skin explants from *Pirt-GCaMP3* DIO mice at 22 weeks of age with an anti-NGF neutralizing antibody (Figures 5A and 5B). Subsequently, we conducted Pirt-GCaMP3 Ca^{2+} imaging to assess sensory axon and terminal activation in response to capsaicin applications (Figure 5B). The capsaicin-mediated hypersensitivity observed in DIO ear skin explants was significantly suppressed by pre-treating the explants with the anti-NGF neutralizing antibody (Figures 5C–5F and S9A–S9D). Among the downstream targets of NGF-TrkA signaling, such as phosphoinositide 3-kinases (PI3K), mitogen-activated protein kinase (MAPK), and phospholipase C (PLC), which are known to be involved in nociceptor sensitization through TRPV1,[28,30,31] we examined whether inhibiting PI3K leads to the blockage of capsaicin-mediated hypersensitivity. To address this, we pre-treated the ear skin from *Pirt-GCaMP3* DIO mice at 22 weeks of age with Wortmannin, a PI3K inhibitor (Figures 5A and 5B). Like the anti-NGF neutralizing antibody treatment, the capsaicin-mediated hypersensitivity observed in DIO ear skin explants was significantly suppressed by pre-treating the explants with Wortmannin (Figures 5G–5J and S9E–S9H). These data suggest that NGF-TrkA-PI3K signaling is necessary for capsaicin-mediated hypersensitivity in the epidermis of DIO ear skin (Figures 5K and S9I). Moreover, this procedure is able to screen small compound inhibitors to suppress the capsaicin-mediated hypersensitivity observed in DIO ear skin explants.

DISCUSSION

We present evidence supporting the role of keratinocyte-derived NGF as a local signal sensitizing the peripheral terminals of nociceptive neurons through NGF-TrkA-PI3K signaling within the epidermis of DIO ear skin, thereby augmenting pain-associated behaviors in response to nociceptive stimuli (Figure 5K). At the mechanistic level, elevated insulin levels enhance *Ngf* expression in primary keratinocytes from the epidermis. Although no significant changes were observed in serum insulin levels in DIO mice between 18 and 22 weeks of age, insulin levels appear to rise sufficiently by 22 weeks of age to induce *Ngf* expression in keratinocytes within the non-capillary epidermis. Considering the increased vascular permeability in DIO ear skin vasculature at 22 weeks of age, but not at 18 weeks of age, one scenario is that the increased vascular permeability may facilitate the diffusion of circulating insulin from dermal capillaries into the non-capillary epidermis in DIO ear skin. In this scenario, reducing or blocking vascular permeability could regulate insulin levels in the epidermis of DIO ear skin, potentially leading to decreased epidermal NGF expression and consequently attenuating sensory hypersensitivity.

The observation that DIO ear skin undergoes axon degeneration in nociceptive neurons within the epidermis at 30 weeks of age raises the intriguing question of what triggers this degeneration. Previous studies have demonstrated that the prolonged activation of nociceptive neurons accelerates axon degeneration in DIO skin.[11] However, the precise mechanisms driving axon degeneration due to the prolonged activation of nociceptive neurons remain incompletely elucidated. In this context, inhibiting the sensitization of nociceptors through targeting local NGF-TrkA-PI3K signaling could potentially prevent axon degeneration in DIO skin.

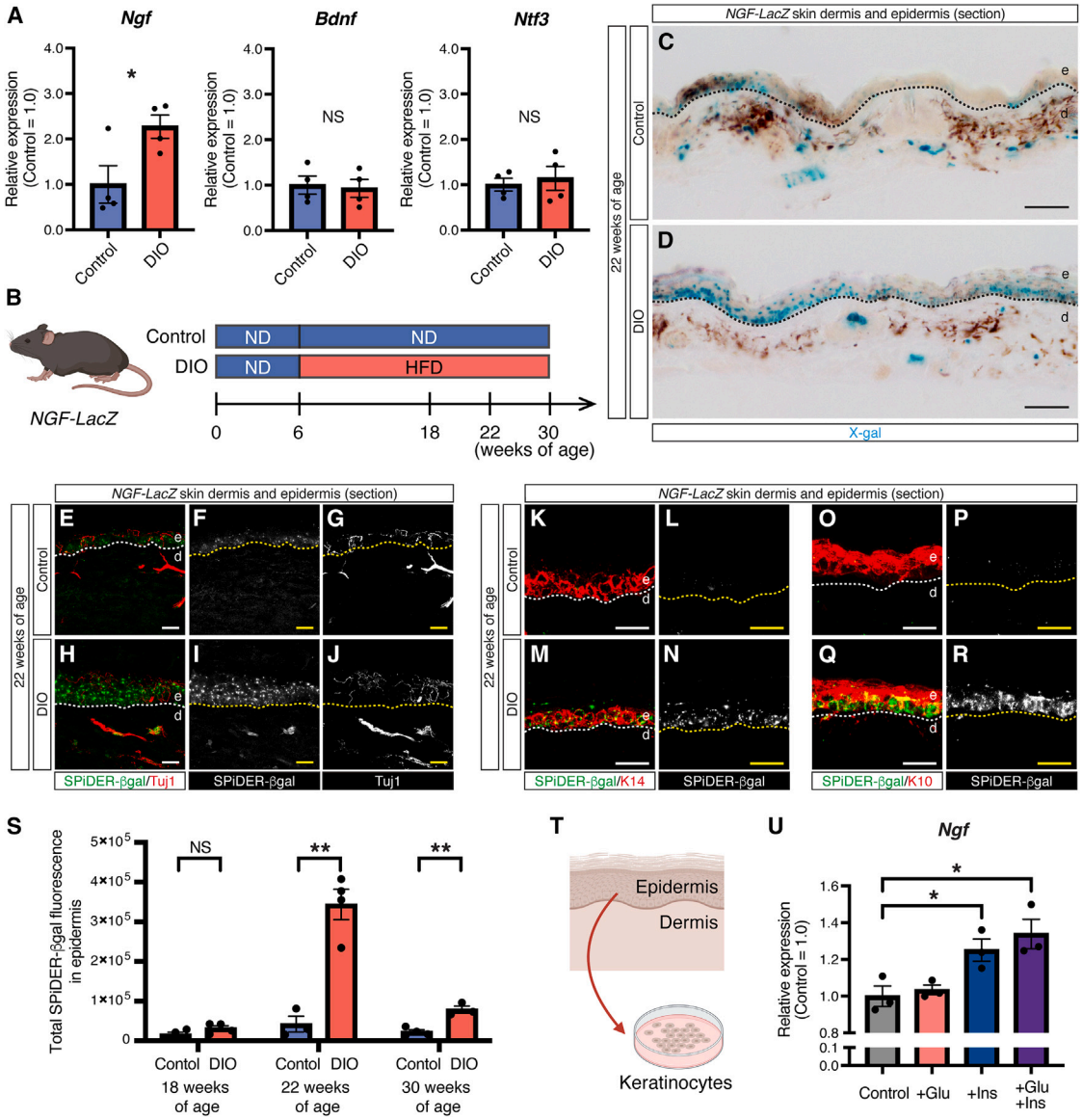

Figure 4. DIO enhances NGF expression in the epidermis

(A) Relative mRNA expression levels of neurotrophic factors (*Ngf*, *Bdnf*, and *Ntf3*) in the epidermis of ear skin from control and DIO mice at 22 weeks of age. Expression levels are normalized by those in the epidermis of ear skin from control mice. $N = 4$ in each group.

(B) Schematic diagram of the induction of DIO in *NGF-LacZ* mice.

(C–D) Representative images of X-gal staining of ear skin sections of *NGF-LacZ* control (C) and DIO mouse (D) at 22 weeks of age (blue). Scale bars: 100 μm

(E–R) Representative double immunofluorescence images of ear skin sections of *NGF-LacZ* control (E-G, K-L, and O-P) and DIO mice (H-J, M-N, and Q-R) at 22 weeks of age. SPiDER-βgal (E, H, K, M, O, and Q, green; F, I, L, N, P, and R, white) together with antibodies to Tuj1 (E and H, red; G and J, white), K14 (K and M, red), or K10 (O and Q, red) were used. Dashed lines (C-R) indicate the border between the epidermis (e) and the dermis (d).

(S) Total SPiDER-βgal fluorescence in the epidermis of ear skin from *NGF-LacZ* mice at 18 weeks of age ($N = 4$ control, $N = 4$ DIO), 22 weeks of age ($N = 3$ control, $N = 4$ DIO), and 30 weeks of age ($N = 4$ control, $N = 3$ DIO).

(T) Schematic diagram of primary mouse keratinocyte culture. Keratinocytes were isolated from adult ear skin and cultured with glucose, insulin, or a combination of both.

(U) Relative *Ngf* mRNA expression levels in primary mouse keratinocytes cultured with glucose (+Glu), insulin (+Ins), or a combination of both (+Glu +Ins). Expression levels are normalized by those in primary mouse keratinocytes cultured without glucose and insulin. $N = 3$ in each group. See also Figures S6, S7, S8, and S10. Results are shown as the mean ± SEM. *$p < 0.05$, **$p < 0.01$; NS, not significant ($p > 0.05$). p values were determined by the parametric two-tailed t test. The schematic diagrams were partially created with BioRender.com.

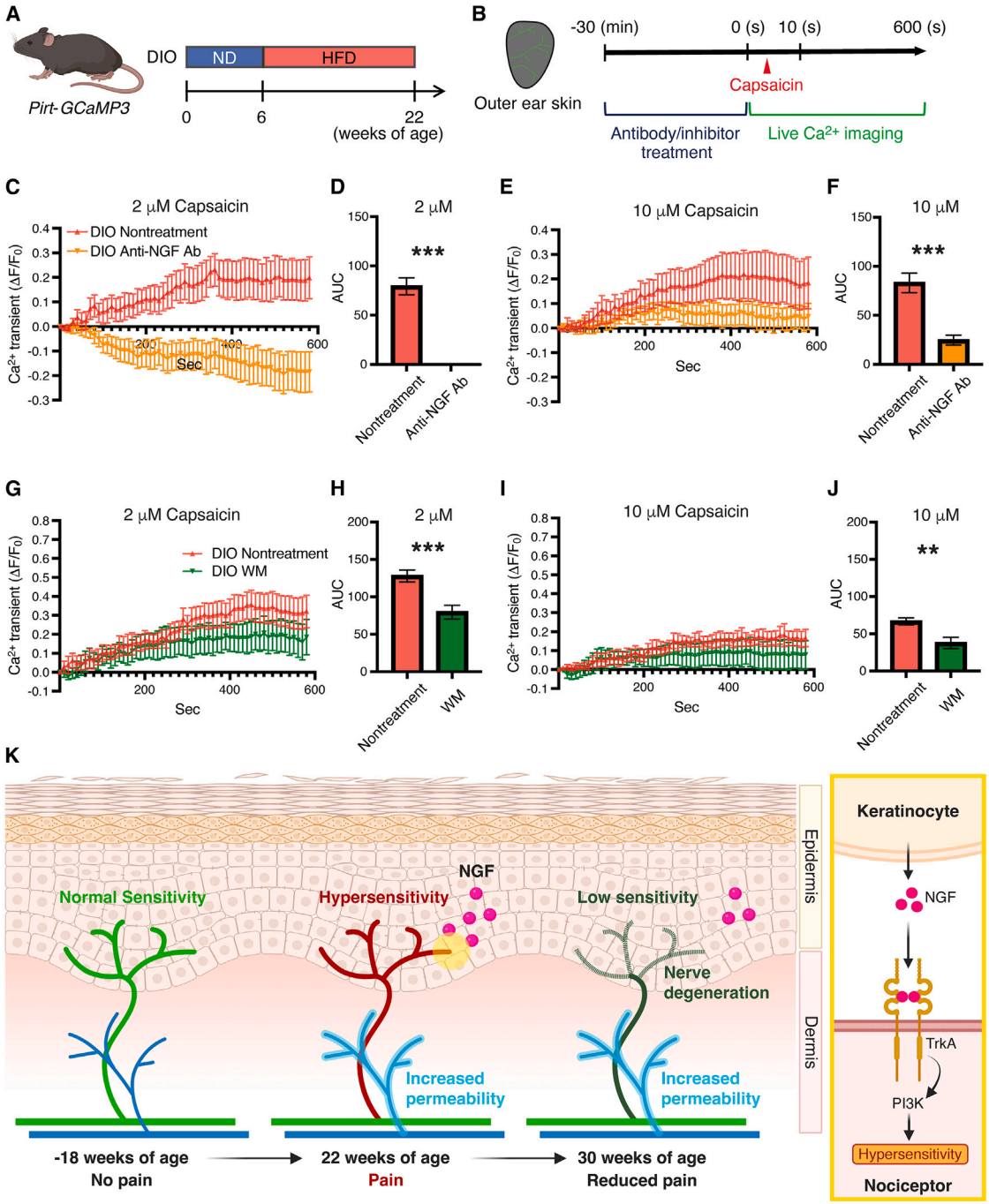

Figure 5. Inhibition of NGF-TrkA-PI3K signaling suppress hypersensitivity in DIO skin

(A) Schematic diagram of the induction of DIO in *Pirt-GCaMP3* mice.

(B) Schematic diagram illustrating *ex vivo* live Pirt-GCaMP3 Ca^{2+} imaging of ear skin explants treated with anti-NGF neutralizing antibody or Wortmannin, a PI3K inhibitor. The ear skin explants from *Pirt-GCaMP3* DIO mice at 22 weeks of age were pre-treated with either anti-NGF neutralizing antibody or Wortmannin for 30 min prior to Pirt-GCaMP3 Ca^{2+} imaging.

(C–J) Quantification of Ca^{2+} responses within the ear skin explants treated with or without anti-NGF neutralized antibody treatment (C-F, Anti-NGF Ab) or Wortmannin treatment (G-J, WM). $N = 6$ in each group. The amplitude of the Ca^{2+} transient was evoked by 2 μM capsaicin (C and G) and 10 μM capsaicin (E and I). Ca transient is normalized by baseline Ca transient ($\Delta F/F_0$). The integrated Ca^{2+} transient ($\Delta F/F_0$) was calculated as AUC (D, F, H, and J). Results are shown as the mean ± SEM. $^{**}p < 0.01$, $^{***}p < 0.001$. *p* values were determined by the parametric two-tailed *t* test.

(K) Graphical summary for pain-associated behaviors, sensory hypersensitivity, epidermal axon projections, vascular permeability, epidermal NGF expression, and keratinocyte-nociceptor interactions in the ear skin of DIO mice. See also Figure S9. The schematic diagrams and graphic summary were partially created with BioRender.com.

We focused our studies on a DIO ear skin model of painful small fiber neuropathy. We assessed pain-associated behaviors, evaluated sensory activity by *ex vivo* Ca^{2+} imaging, and examined axonal changes within the ear skin. Our immunohistochemical analysis of footpad skin indicates that there is no observable difference in skin innervation and vascularization between the ear skin and the footpad skin (Figure S3B versus S10A). Moreover, DIO not only enhances NGF expression in the epidermis of ear skin, but also increases NGF expression in the epidermis of footpad skin at 22 weeks of age (Figures S10B and S10C). These findings suggest that DIO enhances thermal pain behaviors by promoting keratinocyte-derived NGF, which acts as a local signal sensitizing the peripheral terminals of nociceptive neurons through NGF-TrkA-PI3K signaling within the epidermis of DIO footpad skin.

Considering the close proximity of keratinocytes to sensory terminals within the epidermis, it is established that keratinocytes contribute to mechanical, cold and heat sensation by detecting these stimuli and releasing neuroactive molecules for sensory neurons.[32–34] In line with this concept, we present evidence that the crosstalk between keratinocytes and nociceptor terminals plays a crucial role in capsaicin-evoked pain reactions in painful small fiber neuropathy through NGF-TrkA-PI3K signaling. Human clinical trials using recombinant human NGF or Tanezumab, a humanized monoclonal antibody with high selectivity for NGF, in diabetic neuropathy patients have been performed previously with limited effects on pain reduction.[35,36] Our understanding of the local interactions between keratinocytes and nociceptor terminals within the epidermis, along with the identification of potential target signaling pathways such as NGF-TrkA-PI3K signaling to regulate nociceptor sensitization, could serve as the foundation for new therapeutic strategies to manage neuropathic pain in diabetic painful small fiber neuropathy. Importantly, these approaches could be topically applied, potentially circumventing drug side effects associated with systemic interventions.

Limitations of the study

One limitation of this study is our focus on evoked pain by nociceptive stimuli. However, patients with painful small fiber neuropathy suffer from spontaneous ongoing pain in addition to evoked pain. Our *ex vivo* Ca^{2+} imaging system using *Pirt-GCaMP3* may have limitations in detecting spontaneous firing activity due to the relatively slow conformation changes of GCaMP3. Measuring local spontaneous firing activity in nociceptive axons of DIO skin using updated GCaMP proteins such as GCaMP8 represents an essential next step. Another limitation is that this study focused on male mice for DIO studies, as DIO onset in juvenile male mice (6 weeks old) led to a more significant increase in weight gain, glucose levels, and insulin levels compared to female mice. Since most DIO studies initiate the diet in juvenile mice, and considering that males are generally more susceptible to weight gain and elevated glucose and insulin levels,[37,38] we recognize this as a limitation of our study. Since the age at which DIO begins affects sex differences in weight gain, we are exploring the age of DIO onset, which also impacts sex differences in pain behavior and sensory hypersensitivity in our future studies.

RESOURCE AVAILABILITY

Lead contact

Requests for further information and resources should be directed to and will be fulfilled by the lead contact, Yoh-suke Mukouyama (mukoyamay@mail.nih.gov).

Materials availability

This study did not generate new unique materials.

Data and code availability

- All data reported in this article will be shared by the lead contact upon request.
- This article does no report original code.
- Any additional information required to reanalyze the data reported in this article is available from the lead contact upon request.

ACKNOWLEDGMENTS

Thanks to T. Clark and the staff of NIH Bldg50 facility for assistance with mouse breeding and care; E. Tyler and A. Hoofring of NIH medical art branch for schematic illustrations; K. Gill for laboratory management, technical support, and article editing; V. Sam, J.Dawes, and S. Thacker for administrative assistance. Thanks also to members of Laboratory of Stem Cell and Neuro-Vascular Biology for thoughtful discussion and technical help. This work was supported by the Intramural Research Program of the National Heart, Lung, and Blood Institute, National Institutes of Health (HL005702-18 to Y.M.).

AUTHOR CONTRIBUTIONS

Conceptualization: Y.K. and Y.M.; formal analysis: Y.K. and S.S.; funding acquisition: Y.M.; investigation: Y.K. and S.S.; methodology: Y.K. and S.S.; project administration: Y.M.; resources: X.D.; supervision: Y.M.; validation: Y.K. and S.S.; visualization: Y.K. and S.S.; writing - original draft: Y.K. and Y.M.; writing - review and editing: Y.K., S.S., Y.M., and X.D.

DECLARATION OF INTERESTS

The authors declare no competing or financial interests.

STAR★METHODS

Detailed methods are provided in the online version of this paper and include the following:

- KEY RESOURCES TABLE
- EXPERIMENTAL MODEL AND STUDY PARTICIPANT DETAILS
  - Mice
  - Primary mouse keratinocyte culture
- METHOD DETAILS
  - Body weight, blood glucose, and serum insulin measurement
  - Pain behavior assay
  - *Ex vivo* live Ca^{2+} imaging of mouse ear skin
  - Section immunostaining of mouse ear skin
  - Measurement of intraepidermal nerve fiber (IENF) density
  - Measurement of $PLVAP^{+}$ blood vessels
  - Measurement of $CD45^{+}$ immune cells in the epidermis
  - Whole-mount immunostaining of mouse ear skin
  - Quantitative RT-PCR
  - X-gal staining of mouse ear skin
  - SPiDER-βgal staining of mouse ear skin
  - Quantification of SPiDER-βgal signals in epidermis
- QUANTIFICATION AND STATISTICAL ANALYSIS

SUPPLEMENTAL INFORMATION

Supplemental information can be found online at https://doi.org/10.1016/j.isci.2025.112047.

Received: August 12, 2024
Revised: December 2, 2024
Accepted: February 13, 2025
Published: February 17, 2025

REFERENCES

1. Feldman, E.L., Callaghan, B.C., Pop-Busui, R., Zochodne, D.W., Wright, D.E., Bennett, D.L., Bril, V., Russell, J.W., and Viswanathan, V. (2019). Diabetic neuropathy. Nat. Rev. Dis. Primers *5*, 41. https://doi.org/10.1038/s41572-019-0092-1.
2. Vincent, A.M., Callaghan, B.C., Smith, A.L., and Feldman, E.L. (2011). Diabetic neuropathy: cellular mechanisms as therapeutic targets. Nat. Rev. Neurol. *7*, 573–583. https://doi.org/10.1038/nrneurol.2011.137.
3. Divisova, S., Vlckova, E., Hnojcikova, M., Skorna, M., Nemec, M., Dubovy, P., Dusek, L., Jarkovsky, J., Belobradkova, J., and Bednarik, J. (2012). Prediabetes/early diabetes-associated neuropathy predominantly involves sensory small fibres. J. Peripher. Nerv. Syst. *17*, 341–350. https://doi.org/10.1111/j.1529-8027.2012.00420.x.
4. Suzuki, Y., Sato, J., Kawanishi, M., and Mizumura, K. (2002). Lowered response threshold and increased responsiveness to mechanical stimulation of cutaneous nociceptive fibers in streptozotocin-diabetic rat skin in vitro–correlates of mechanical allodynia and hyperalgesia observed in the early stage of diabetes. Neurosci. Res. *43*, 171–178. https://doi.org/10.1016/s0168-0102(02)00033-0.
5. Devigili, G., Tugnoli, V., Penza, P., Camozzi, F., Lombardi, R., Melli, G., Broglio, L., Granieri, E., and Lauria, G. (2008). The diagnostic criteria for small fibre neuropathy: from symptoms to neuropathology. Brain *131*, 1912–1925. https://doi.org/10.1093/brain/awn093.
6. Pham, M., Oikonomou, D., Hornung, B., Weiler, M., Heiland, S., Bäumer, P., Kollmer, J., Nawroth, P.P., and Bendszus, M. (2015). Magnetic resonance neurography detects diabetic neuropathy early and with Proximal Predominance. Ann. Neurol. *78*, 939–948. https://doi.org/10.1002/ana.24524.
7. Jende, J.M.E., Kender, Z., Rother, C., Alvarez-Ramos, L., Groener, J.B., Pham, M., Morgenstern, J., Oikonomou, D., Hahn, A., Juerchott, A., et al. (2020). Diabetic Polyneuropathy Is Associated With Pathomorphological Changes in Human Dorsal Root Ganglia: A Study Using 3T MR Neurography. Front. Neurosci. *14*, 570744. https://doi.org/10.3389/fnins.2020.570744.
8. Nowicki, M., Kosacka, J., Serke, H., Blüher, M., and Spanel-Borowski, K. (2012). Altered sciatic nerve fiber morphology and endoneural microvessels in mouse models relevant for obesity, peripheral diabetic polyneuropathy, and the metabolic syndrome. J. Neurosci. Res. *90*, 122–131. https://doi.org/10.1002/jnr.22728.
9. Thrainsdottir, S., Malik, R.A., Dahlin, L.B., Wiksell, P., Eriksson, K.F., Rosén, I., Petersson, J., Greene, D.A., and Sundkvist, G. (2003). Endoneurial capillary abnormalities presage deterioration of glucose tolerance and accompany peripheral neuropathy in man. Diabetes *52*, 2615–2622. https://doi.org/10.2337/diabetes.52.10.2615.
10. Wang, L., Chopp, M., Szalad, A., Jia, L., Lu, X., Lu, M., Zhang, L., Zhang, Y., Zhang, R., and Zhang, Z.G. (2015). Sildenafil ameliorates long term peripheral neuropathy in type II diabetic mice. PLoS One *10*, e0118134. https://doi.org/10.1371/journal.pone.0118134.
11. Jayaraj, N.D., Bhattacharyya, B.J., Belmadani, A.A., Ren, D., Rathwell, C.A., Hackelberg, S., Hopkins, B.E., Gupta, H.R., Miller, R.J., and Menichella, D.M. (2018). Reducing CXCR4-mediated nociceptor hyperexcitability reverses painful diabetic neuropathy. J. Clin. Investig. *128*, 2205–2225. https://doi.org/10.1172/JCI92117.
12. Pham, V.M., Tu, N.H., Katano, T., Matsumura, S., Saito, A., Yamada, A., Furue, H., and Ito, S. (2018). Impaired peripheral nerve regeneration in type-2 diabetic mouse model. Eur. J. Neurosci. *47*, 126–139. https://doi.org/10.1111/ejn.13771.
13. Bonomo, R., Kramer, S., and Aubert, V.M. (2022). Obesity-Associated Neuropathy: Recent Preclinical Studies and Proposed Mechanisms. Antioxidants Redox Signal. *37*, 597–612. https://doi.org/10.1089/ars.2021.0278.
14. Burgess, J., Frank, B., Marshall, A., Khalil, R.S., Ponirakis, G., Petropoulos, I.N., Cuthbertson, D.J., Malik, R.A., and Alam, U. (2021). Early Detection of Diabetic Peripheral Neuropathy: A Focus on Small Nerve Fibres. Diagnostics *11*, 165. https://doi.org/10.3390/diagnostics11020165.
15. Stino, A.M., and Smith, A.G. (2017). Peripheral neuropathy in prediabetes and the metabolic syndrome. J. Diabetes Investig. *8*, 646–655. https://doi.org/10.1111/jdi.12650.
16. Pan, H., Fatima, M., Li, A., Lee, H., Cai, W., Horwitz, L., Hor, C.C., Zaher, N., Cin, M., Slade, H., et al. (2019). Identification of a Spinal Circuit for Mechanical and Persistent Spontaneous Itch. Neuron *103*, 1135–1149. https://doi.org/10.1016/j.neuron.2019.06.016.
17. Shimada, S.G., and LaMotte, R.H. (2008). Behavioral differentiation between itch and pain in mouse. Pain *139*, 681–687. https://doi.org/10.1016/j.pain.2008.08.002.
18. Kim, Y.S., Chu, Y., Han, L., Li, M., Li, Z., LaVinka, P.C., Sun, S., Tang, Z., Park, K., Caterina, M.J., et al. (2014). Central terminal sensitization of TRPV1 by descending serotonergic facilitation modulates chronic pain. Neuron *81*, 873–887. https://doi.org/10.1016/j.neuron.2013.12.011.
19. Yamazaki, T., Li, W., Yang, L., Li, P., Cao, H., Motegi, S.I., Udey, M.C., Bernhard, E., Nakamura, T., and Mukouyama, Y.S. (2018). Whole-Mount Adult Ear Skin Imaging Reveals Defective Neuro-Vascular Branching Morphogenesis in Obese and Type 2 Diabetic Mouse Models. Sci. Rep. *8*, 430. https://doi.org/10.1038/s41598-017-18581-7.
20. Ono, S., Egawa, G., and Kabashima, K. (2017). Regulation of blood vascular permeability in the skin. Inflamm. Regen. *37*, 11. https://doi.org/10.1186/s41232-017-0042-9.
21. Denzer, L., Muranyi, W., Schroten, H., and Schwerk, C. (2023). The role of PLVAP in endothelial cells. Cell Tissue Res. *392*, 393–412. https://doi.org/10.1007/s00441-023-03741-1.
22. Jain, A., Hakim, S., and Woolf, C.J. (2024). Immune drivers of physiological and pathological pain. J. Exp. Med. *221*, e20221687. https://doi.org/10.1084/jem.20221687.
23. Skaper, S.D. (2018). Neurotrophic Factors: An Overview. Methods Mol. Biol. *1727*, 1–17. https://doi.org/10.1007/978-1-4939-7571-6_1.
24. Barker, P.A., Mantyh, P., Arendt-Nielsen, L., Viktrup, L., and Tive, L. (2020). Nerve Growth Factor Signaling and Its Contribution to Pain. J. Pain Res. *13*, 1223–1241. https://doi.org/10.2147/jpr.S247472.
25. Chang, D.S., Hsu, E., Hottinger, D.G., and Cohen, S.P. (2016). Anti-nerve growth factor in pain management: current evidence. J. Pain Res. *9*, 373–383. https://doi.org/10.2147/JPR.S89061.
26. Denk, F., Bennett, D.L., and McMahon, S.B. (2017). Nerve Growth Factor and Pain Mechanisms. Annu. Rev. Neurosci. *40*, 307–325. https://doi.org/10.1146/annurev-neuro-072116-031121.
27. Lawrence, G.W., Zurawski, T.H., and Dolly, J.O. (2021). Ca(2+) Signalling Induced by NGF Identifies a Subset of Capsaicin-Excitable Neurons Displaying Enhanced Chemo-Nociception in Dorsal Root Ganglion Explants from Adult pirt-GCaMP3 Mouse. Int. J. Mol. Sci. *22*, 2589. https://doi.org/10.3390/ijms22052589.
28. Stratiievska, A., Nelson, S., Senning, E.N., Lautz, J.D., Smith, S.E., and Gordon, S.E. (2018). Reciprocal regulation among TRPV1 channels and phosphoinositide 3-kinase in response to nerve growth factor. Elife *7*, e38869. https://doi.org/10.7554/eLife.38869.
29. Reichert, O., Fleming, T., Neufang, G., Schmelz, M., Genth, H., Kaever, V., Wenck, H., Stäb, F., Terstegen, L., Kolbe, L., and Roggenkamp, D. (2017). Impaired glyoxalase activity is associated with reduced expression of

neurotrophic factors and pro-inflammatory processes in diabetic skin cells. Exp. Dermatol. *26*, 44–50. https://doi.org/10.1111/exd.13118.

30. Ji, R.-R., Samad, T.A., Jin, S.-X., Schmoll, R., and Woolf, C.J. (2002). p38 MAPK Activation by NGF in Primary Sensory Neurons after Inflammation Increases TRPV1 Levels and Maintains Heat Hyperalgesia. Neuron *36*, 57–68. https://doi.org/10.1016/S0896-6273(02)00908-X.
31. Chuang, H.-h., Prescott, E.D., Kong, H., Shields, S., Jordt, S.-E., Basbaum, A.I., Chao, M.V., and Julius, D. (2001). Bradykinin and nerve growth factor release the capsaicin receptor from PtdIns(4,5)P2-mediated inhibition. Nature *411*, 957–962. https://doi.org/10.1038/35082088.
32. Sadler, K.E., Moehring, F., and Stucky, C.L. (2020). Keratinocytes contribute to normal cold and heat sensation. Elife *9*, e58625. https://doi.org/10.7554/eLife.58625.
33. Mikesell, A.R., Isaeva, O., Moehring, F., Sadler, K.E., Menzel, A.D., and Stucky, C.L. (2022). Keratinocyte PIEZO1 modulates cutaneous mechanosensation. Elife *11*, e65987. https://doi.org/10.7554/eLife.65987.
34. Moehring, F., Cowie, A.M., Menzel, A.D., Weyer, A.D., Grzybowski, M., Arzua, T., Geurts, A.M., Palygin, O., and Stucky, C.L. (2018). Keratinocytes mediate innocuous and noxious touch via ATP-P2X4 signaling. Elife *7*, e31684. https://doi.org/10.7554/eLife.31684.
35. Apfel, S.C., Schwartz, S., Adornato, B.T., Freeman, R., Biton, V., Rendell, M., Vinik, A., Giuliani, M., Stevens, J.C., Barbano, R., and Dyck, P.J. (2000). Efficacy and safety of recombinant human nerve growth factor in patients with diabetic polyneuropathy: A randomized controlled trial. rhNGF Clinical Investigator Group. JAMA *284*, 2215–2221. https://doi.org/10.1001/jama.284.17.2215.
36. Bramson, C., Herrmann, D.N., Carey, W., Keller, D., Brown, M.T., West, C.R., Verburg, K.M., and Dyck, P.J. (2015). Exploring the role of tanezumab as a novel treatment for the relief of neuropathic pain. Pain Med. *16*, 1163–1176. https://doi.org/10.1111/pme.12677.
37. Salinero, A.E., Anderson, B.M., and Zuloaga, K.L. (2018). Sex differences in the metabolic effects of diet-induced obesity vary by age of onset. Int. J. Obes. *42*, 1088–1091. https://doi.org/10.1038/s41366-018-0023-3.
38. Huang, K.P., Ronveaux, C.C., Knotts, T.A., Rutkowsky, J.R., Ramsey, J.J., and Raybould, H.E. (2020). Sex differences in response to short-term high fat diet in mice. Physiol. Behav. *221*, 112894. https://doi.org/10.1016/j.physbeh.2020.112894.
39. Liu, Y., Rutlin, M., Huang, S., Barrick, C.A., Wang, F., Jones, K.R., Tessarollo, L., and Ginty, D.D. (2012). Sexually dimorphic BDNF signaling directs sensory innervation of the mammary gland. Science *338*, 1357–1360. https://doi.org/10.1126/science.1228258.
40. Lichti, U., Anders, J., and Yuspa, S.H. (2008). Isolation and short-term culture of primary keratinocytes, hair follicle populations and dermal cells from newborn mice and keratinocytes from adult mice for in vitro analysis and for grafting to immunodeficient mice. Nat. Protoc. *3*, 799–810. https://doi.org/10.1038/nprot.2008.50.
41. Zimmermann, K., Hein, A., Hager, U., Kaczmarek, J.S., Turnquist, B.P., Clapham, D.E., and Reeh, P.W. (2009). Phenotyping sensory nerve endings in vitro in the mouse. Nat. Protoc. *4*, 174–196. https://doi.org/10.1038/nprot.2008.223.
42. Yamazaki, T., Li, W., and Mukouyama, Y.S. (2018). Whole-mount Confocal Microscopy for Adult Ear Skin: A Model System to Study Neuro-vascular Branching Morphogenesis and Immune Cell Distribution. J. Vis. Exp. *133*, 57406. https://doi.org/10.3791/57406.

STAR★METHODS

KEY RESOURCES TABLE

REAGENT or RESOURCE	SOURCE	IDENTIFIER
Antibodies		
Anti-NGF neutralized antibody	exalpha	L146M
Mouse anti-Tuj1 (Tubulin b3, TUBB3) antibody	BioLegend	801202; RRID: AB_2313773
Goat anti-TrkA antibody	R&D Systems	AF1056-SP; RRID: AB_2283049
Goat anti-TrkB antibody	R&D Systems	AF1494-SP; RRID: AB_2155264
Goat anti-TrkC antibody	R&D Systems	AF1404-SP; RRID: AB_2155412
Chick anti-GFP antibody	abcam	ab13970; RRID: AB_300798
Rabbit anti-MBP (Myelin Basic Protein) antibody	abcam	ab40390; RRID: AB_1141521
Rabbit anti-K10 (Keratin 10) antibody	BioLegend	905403; RRID: AB_2749902
Guinea pig anti-K14 (Keratin 14) antibody	PROGEN	GP-CK14; RRID: AB_2920669
Armenian hamster anti-PECAM-1 antibody	Millipore Sigma	MAB1398Z; RRID: AB_94207
Rat anti-PLVAP antibody	BD Biosciences	553849; RRID: AB_395086
Rat anti-CD45 antibody	eBioscience	140451–85
Alexa 488-conjugated Mouse anti-Tuj1 (Tubulin b3, TUBB3) antibody	BioLegend	801203; RRID: AB_2564757
Cy3-conjugated Mouse anti-αSMA antibody	Sigma	C6198; RRID: AB_476856
Rabbit anti-SM22a antibody	abcam	ab14106; RRID: AB_443021
Goat anti-Mouse IgG2a, Alexa Fluor 488	Thermo Fisher Scientific	A21131; RRID: AB_2535771
Goat anti-Mouse IgG2a, Alexa Fluor 568	Thermo Fisher Scientific	A21134; RRID: AB_2535773
Goat anti-Mouse IgG2a, Alexa Fluor 633	Thermo Fisher Scientific	A21136; RRID: AB_2535775
Goat anti-Rabbit IgG, Alexa Fluor 568	Thermo Fisher Scientific	A11011; RRID: AB_143157
Goat anti-Rabbit IgG, Alexa Fluor 647	Jackson ImmunoResearch	111-605-144; RRID: AB_2338078
Goat anti-Rat IgG, Alexa Fluor 568	Thermo Fisher Scientific	A11077; RRID: AB_2534121
Goat anti-Armenian Hamster IgG, Alexa Fluor 647	Jackson ImmunoResearch	127-605-160; RRID: AB_2339001
Goat anti-Guinea Pig IgG, Alexa Fluor 488	Jackson ImmunoResearch	106-546-003; RRID: AB_2337441
Goat anti-Guinea Pig IgG, Alexa Fluor 647	Jackson ImmunoResearch	106-605-003; RRID: AB_2337446
Donkey anti-Goat IgG, Alexa Fluor 633	Thermo Fisher Scientific	A21082; RRID: AB_10562400
Chemicals, peptides, and recombinant proteins		
High-fat diet	Research Diets	D12492
Glucose solution	Thermo Fisher Scientific	A2494001
Insulin, human recombinant	Thermo Fisher Scientific	12585014
Wortmannin	Sigma	W1628
Capsaicin	Sigma	M2028
KCl	Mallinckrodt	6858
Ambion DNase I	Thermo Fisher Scientific	AM2222
SPiDER-βgal	Dojindo	SG02
Critical commercial assays		
AlphaTrak 3 blood glucose monitoring system	Zoetis	N/A
RNeasy Mini kits	QUAGEN	N/A
SuperScript III First-Strand Synthesis SuperMix	Thermo Fisher Scientific	18080400
THUNDERBIRD Next SYBR qPCR Mix	TOYOBO	N/S
Experimental models: Organisms/strains		
Mouse: C57BL/6J	The Jackson Laboratory	000664
Mouse: *Pirt-GCaMP3*	Kim et al.[18]	N/A

(*Continued on next page*)

Continued

REAGENT or RESOURCE	SOURCE	IDENTIFIER
Mouse: *NGF-LacZ*	Liu et al.[39]	N/A
Oligonucleotides		
Primers for quantitative RT-PCR, see Table S1	N/A	N/A
Software and algorithms		
ImageJ	NIH	https://imagej.net/ij/
LightCycler 96 software	Roche	N/A
Prism 10	GraphPad	https://www.graphpad.com/
BioRender	BioRender	https://www.biorender.com/
Other		
Tissue path Superfrost Plus Gold Slides	Fisher Scientific	15-188-48
Leica TCS SP5 confocal	Leica	N/A

EXPERIMENTAL MODEL AND STUDY PARTICIPANT DETAILS

Mice

All animal procedures were approved by the National Heart, Lung, and Blood institute (NHLBI) Animal Care and Use Committee in accordance with National Institutes of Health (NIH) research guidelines for the care and use laboratory animals. The following mice were used in this study: C57BL/6J mice (The Jackson Laboratory), *Pirt-GCaMP3* mice,[18] and *NGF-LacZ* mice.[39] C57BL/6J, *Pirt-GCaMP3* heterozygous, and *NGF-LacZ* heterozygous male mice were randomly separated into two groups and fed either a high-fat diet (60% fat, 20% protein, and 20% carbohydrate kcal; Research Diets, D12492) to induce DIO or a normal diet (10% fat, 20% protein, and 70% carbohydrate kcal) for control from 6 weeks of age with free access to water.

Primary mouse keratinocyte culture

Primary mouse keratinocytes were isolated from C57BL/6J male mice according to the previously established protocol.[40] Isolated mouse keratinocytes were cultured on fibronectin/collagen coated plates at a density of 1,000,000 cells/cm^2. Cells were replated at day 2 to culture under high-glucose (2 mg/mL, ThermoFisher, A2494001) or high-insulin (40 μg/mL, ThermoFisher, 12585014) condition for 2 days. Cells were cultured in a 5% CO2, 20% O2 environment at 37°C.

METHOD DETAILS

Body weight, blood glucose, and serum insulin measurement

Body weights of all mice were measured weekly at the same time of the day. Blood glucose levels were measured using a glucose meter, AlphaTrak 3 blood glucose monitoring system (Zoetis) after 4–6 h fasting. Blood samples were collected after cardiac puncture. Serum insulin levels were measured by Mouse Ultrasensitive Insulin ELISA system (ALPCO) according to manufacturer's protocol.

Pain behavior assay

The control or DIO mice were placed in the plastic clear test chamber and habituated for 10 min. The 10 μL capsaicin solution (0.1 mM in ethanol, Sigma, M2028) was applied into the skin behind the ear after habituation. The mouse behavior was videorecorded for 10 min. The wiping responses with a forelimb toward the stimulus site was manually counted based on the recorded videos. Wiping bouts/600 s were calculated for comparison between control and DIO mice at each stage.

Ex vivo live Ca^{2+} imaging of mouse ear skin

Pirt-GCaMP3 mice at 18, 22, and 30 weeks of age were sacrificed by CO_2 asphyxiation. Ear skin was acutely dissected from *Pirt-GCaMP3* mice, and then the outer ear skin was isolated for Ca^{2+} imaging. Epidermal branched axons located within 20 μm from the surface of hairy skin were imaged. Skin explants were placed in test chamber filled with synthetic interstitial fluid (SIF)[41] and maintained at room temperature. The skin explants were treated with anti-NGF neutralized antibody (0.02 mg/mL, exalpha, L146M) or Wortmannin (1 μM, Sigma, W1628) for 30 min at room temperature before Ca^{2+} imaging. Ca^{2+} imaging was carried out on a Leica TCS SP5 confocal (Leica) with perfusion of SIF. The skin was stimulated by 2 μM or 10 μM Capsaicin (Sigma, M2028) or 20 mM KCl (Mallinckrodt, 6858) and then imaged for 10 min to measure GCaMP3 fluorescent levels. The 5 z stack images were acquired every 10 s. For quantification, time-course images were imported into ImageJ (NIH) to create maximum intensity projection (MIP) images. Three areas with GCaMP3 positive sensory axons were cropped from the MIP images, and averaged Ca^{2+} transients

($\Delta F/F_0$) were calculated. For comparison of sensory activities in response to capsaicin between control and DIO mice, amount of Ca^{2+} transient that was calculated as area under curve was determined.

Section immunostaining of mouse ear skin

Outer ear skin was dissected from adult mice, fixed with 4% paraformaldehyde/PBS at 4°C overnight, sunk in 30% sucrose/PBS at 4°C, and then embedded in OCT compound. Tissues were cryosectioned at 20 μm thickness and collected on pre-cleaned slides (Fisher Scientific, 15-188-48). The samples were incubated in blocking buffer (0.2% Triton X-100, 10% heat inactivated goat or donkey serum in PBS), with diluted primary antibodies 4°C overnight. Staining was performed using Mouse anti-Tuj1 (Tubulin b3, TUBB3) antibody (BioLegend, 801202, 1:200), Goat anti-TrkA antibody (R&D Systems, AF1056-SP, 1:100), Goat anti-TrkB antibody (R&D Systems, AF1494-SP, 1:100), and Goat anti-TrkC antibody (R&D Systems, AF1404-SP, 1:100) to detect axons, Chick anti-GFP antibody (abcam, ab13970, 1:300) to detect GCaMP3 protein in sensory axons, Rabbit anti-MBP (Myelin Basic Protein) antibody (abcam, ab40390, 1:200) to detect myelin membrane in peripheral nerves, Rabbit anti-K10 (Keratin 10) antibody (BioLegend, 905403, 1:400) and Guinea pig anti-K14 (Keratin 14) antibody (PROGEN, GP-CK14, 1:100) to detect keratinocytes, Armenian hamster anti-PECAM-1 antibody (Millipore Sigma, MAB1398Z, 1:300) and Rat anti-PLVAP antibody (BD Biosciences, 553849, 1:100) to detect endothelial cells, and Rat anti-CD45 antibody (eBioscience, 140451-85, 1:100) to detect hematopoietic cells. For immunofluorescent detection, the samples were incubated in blocking buffer containing either Alexa 488-, Alexa 568-, Alexa 633-, or Alexa 647-conjugated secondary antibodies (Jackson ImmunoResearch or Thermo Fisher Scientific, 1:250). All confocal microscopy was carried out on a Leica TCS SP5 confocal (Leica).

Measurement of intraepidermal nerve fiber (IENF) density

IENF was quantified by counting the number of sensory axons crossing the epidermal-dermal junction. The linear IENF density was calculated and expressed as the number of fibers per millimeter of epidermal length (IENF/mm) for the comparison between control and DIO mice.

Measurement of PLVAP$^+$ blood vessels

Area of PLVAP$^+$ blood vessels were quantified using ImageJ (NIH). The percentage of PLVAP$^+$ blood vessels was based on the area of PLVAP$^+$ blood vessels within the area of PECAM-1$^+$ blood vessels.

Measurement of CD45$^+$ immune cells in the epidermis

The quantity of CD45$^+$ immune cells present in the epidermis was counted and expressed as the cell number per millimeter of epidermal length for the comparison between control and DIO mice.

Whole-mount immunostaining of mouse ear skin

Staining was performed essentially as described previously.[19,42] After fixation, connective tissues and fat were removed from the dermal side of the ear skin before staining. The samples were incubated in blocking buffer with diluted primary antibodies 4°C overnight. Staining was performed using Alexa 488-conjugated Mouse anti-Tuj1 (Tubulin b3, TUBB3) antibody (BioLegend, 801203, 1:200) to detect axons, Cy3-conjugated Mouse anti-αSMA antibody (Sigma, C6198, 1:250) and Rabbit anti-SM22a antibody (abcam, ab14106, 1:500) to detect smooth muscle cells, and Armenian hamster anti-PECAM-1 antibody (Millipore Sigma, MAB1398Z, 1:300) to detect endothelial cells. For immunofluorescent detection, the samples were incubated in blocking buffer containing either Alexa 488-, Alexa 568-, or Alexa 647-conjugated secondary antibodies (Jackson ImmunoResearch or Thermo Fisher Scientific, 1:250). All confocal microscopy was carried out on a Leica TCS SP5 confocal (Leica).

Quantitative RT-PCR

Ear skin was incubated in 0.15% Trypsin-EDTA for 45 min at 37°C to separate the epidermis from dermis. Total RNAs from epidermis tissue and primary cultured mouse keratinocytes were extracted using RNeasy Mini kits (QUAGEN) according to the manufacturer's protocol. Residual genomic DNA was digested with Ambion DNase I (Thermo Fisher Scientific, AM2222). First-strand cDNA was synthesized using the SuperScript III First-Strand Synthesis SuperMix (Thermo Fisher Scientific, 18080400). Quantitative RT-PCR was performed using THUNDERBIRD Next SYBR qPCR Mix (TOYOBO). All data of quantitative RT-PCR were calculated using the ddCt method with *Gapdh* as normalization controls. Primers are listed in Table S1.

X-gal staining of mouse ear skin

Outer ear skin was fixed with 0.25% glutaraldehyde/PBS for 30 min on ice. After fixation, connective tissues and fat were removed from the dermal side of the ear skin before staining. The tissues were incubated in 1 mg/mL X-gal overnight at 4°C. The tissues were washed with PBS and post-fixed with 4% paraformaldehyde/PBS. For the section imaging, tissues were further sunk in 30% sucrose/PBS at 4°C and then embedded in OCT compound. Tissues were cryosectioned at 20 μm thickness.

SPiDER-βgal staining of mouse ear skin

Outer ear skin isolated from adult mice was incubated in 20 μM SPiDER-βgal (Dojindo, SG02) for 1 h at 37°C. Tissues were washed with PBS and then fixed with 4% paraformaldehyde/PBS for 1 h on ice. Tissues were further stained together with antibodies as described above.

Quantification of SPiDER-βgal signals in epidermis

Total SPiDER-βgal signals were quantified using ImageJ (NIH). Fluorescent levels were normalized by the area of epidermis in each image.

QUANTIFICATION AND STATISTICAL ANALYSIS

For quantification, we used ImageJ (NIH) for image data and LightCycler 96 software (Roche) for quantitative RT-PCR. Statistical analysis was performed using Prism software. Results were presented as the mean ± SEM. p values were determined by the parametric two-tailed t test. $p < 0.05$ was considered statistically significant. Statistical details of each experiment can be found in the figure legends.